Preprints.org

Article

Improving Device-to-Device Reproducibility of Light-Emitting Diodes Based on Layered Halide Perovskites

Quang-Huy Do , Rémi Antony , Bernard Ratier , Johann Bouclé [*]

Article

Improving Device-to-Device Reproducibility of Light-Emitting Diodes Based on Layered Halide Perovskites

Quang-Huy Do [1], Rémi Antony [1], Bernard Ratier [1] and Johann Bouclé [1,*]

[1]   XLIM UMR 7252, University of Limoges / CNRS, Limoges, 87000, France
*   Correspondence: johann.boucle@unilim.fr; Tel.: +33 5 87 50 67 62

Abstract: Layered halide perovskites have emerged as a promising contender in solid-state lighting thanks to their tunable bandgap, high luminescence quantum yield, and high color purity. However, the fabrication of perovskite light-emitting devices in laboratories usually experiences low device-to-device reproducibility since perovskite crystallization is highly sensitive to ambient conditions, such as humidity and temperature. Although device processing inside gloveboxes is primarily used to reduce the influence of oxygen and moisture, several extraneous variables, including gaseous pollution traces and thermal fluctuations in the inert atmosphere or contaminations from residual solvents confined in the enclosed environment, can destabilize the crystallization process and alter the properties of the emissive layers. Here, we examine different experimental set-ups for spin-coating deposition of layered perovskites in inert atmospheres and their influences on the formation of polycrystalline thin films. Our results demonstrate that fluctuations in the glovebox properties (concentrations of residual O_2 and H_2O or solvent traces), even in very short timescales, can negatively impact the consistency of the perovskite film formation, while thermal variation plays a relatively minor role in this phenomenon. Furthermore, careful storage of chemical species inside the workstation is critical for reproducing high-quality perovskite layers. Consequently, when applying our most controlled environment for perovskite deposition, the photoluminescence lifetime of perovskite thin films shows a standard deviation of only 3%, whereas the reference set-up yields a 15% standard deviation. Regarding complete perovskite light-emitting diodes, the uncertainties in statistical luminance and EQE data are significantly reduced from 230% and 140% to 38% and 42%, respectively.

Keywords: layered halide perovskites; perovskite light-emitting diodes (PeLED); quasi-2D; device-to-device reproducibility

1. Introduction

Halide perovskites have emerged in recent years as promising cost-effective alternatives to III-V semiconductors in optoelectronics, from solar cells [1,2], photodetectors [3], to light-emitting diodes (LEDs) [4–6]. While possessing a high optical absorption coefficient associated with a direct transition and a proficient charge carrier mobility with large diffusion length suitable for photovoltaic and photo-sensing applications, halide perovskites also offer outstanding emission efficiencies, relatively high color purity and a controllable emission bandgap, which are crucial features for LEDs. With full width at half maximum (FWHM) as narrow as 18 nm, 23 nm, and 35 nm, respectively, for red, green, and blue emitters [7–9], together with the ability to tune emission wavelengths on demand [10], PeLEDs are expected to shortly replace organic and quantum dot LEDs in the high-resolution display market.

After the demonstration of working PeLEDs based on three-dimensional halide perovskites at room temperature by Tan et al. in 2014 [11], numerous studies have been conducted to promote the rapid evolution of these devices in terms of luminance and efficiency. Generally, PeLEDs can be

classified by the dimensionality of the perovskite materials, including 3D perovskites, quasi-2D (or layered or multi-dimensional) perovskites, and perovskite quantum dots. Among these, the quasi-2D has been the focus of attention thanks to their unique structure, which features alternately-aligned thin layers of inorganic halide sheets and organic ammonium cation spacers, forming an inherent multiple-quantum-well structure [12–14]. This structure allows for enhanced confinement of excitons via quantum and dielectric effects to induce efficient radiative recombination [15]. Another distinctive characteristic of layered perovskites is the formation of different phases in polycrystalline thin films (usually inscribed by n = 1 for the 2D phase, n = 2, 3, 4, etc… for the quasi-2D phases, and n = ∞ for the 3D phase) and the funnelling of charge carriers from the low-n phases with large bandgaps to the high-n phases with smaller bandgaps, capable of passivating non-radiative structural defects [16,17]. The first use of layered perovskites in PeLEDs at ambient temperature could be traced back to 2016 when Byun et al. fabricated a green PeLED based on $PEA_2MA_{n-1}Pb_nBr_{3n+1}$ with a maximum luminance of 8,400 cd/m² [18]. Since then, most studies have focused on improving either the luminous intensity of the devices or their external quantum efficiencies (EQE). For example, the brightest green quasi-2D PeLED that has been published showed a luminance of 91,000 cd/m² at EQE of 16% [19]. Conversely, the efficiency record was obtained at 28% by Liu et al. after a dual-additive treatment of the bromide perovskite active layer [20].

Despite that the brightness and efficiency of PeLEDs have matched those of commercial LEDs [21], large-scale production of this technology is still challenging, in which a low rate of device reproducibility is of critical concern. In layered perovskites, this reproducibility problem arises from the fact that the n phases have minimal differences in their formation energies [22], resulting in large variations in the phase composition even when a slight change in perovskite thin-film growth conditions occurs [23,24]. Factors contributing to the crystallization of layered perovskites can be categorized into controllable and extraneous variables. Controllable variables include the choice of organic ligands [23,25–27], precursor preparation methods [28,29], growth methods [30,31], use of antisolvents and additives [20,26,32–34]. Extraneous variables comprise environmental factors such as ambient temperature and humidity. For example, changes in room temperature during daytime or climate between seasons can entail noticeable deviations in perovskite crystallization and, thus in device performance [24,35]. For this reason, most manipulation of layered perovskites would be prepared under glovebox conditions with controlled O_2 and H_2O levels. However, even an inert environment can still be prone to instability because of unintentional gas or temperature fluctuation, caused by manipulation of the researchers and the functioning of equipment, as well as contaminations from chemical species and solvents stored in the glovebox (particularly when the glovebox needs to be shared amongst several users).

Therefore, this report aims at shedding light on the influences of extrinsic factors in deposition set-ups under glovebox environments on the properties of quasi-2D perovskites and the performance of optoelectronic devices based on them. Our observations revealed that fluctuations in the concentration of oxygen and moisture, as well as untraceable chemical contamination during perovskite casting, noticeably altered the phase composition and optical properties of the multi-dimensional perovskite layers, leading to reduced reproducibility of PeLEDs. Furthermore, regular regeneration of the glovebox, with careful attention paid to chemical storage, can reduce the standard deviations (std) in the PeLED performance by up to six times while improving the optical properties of the polycrystalline perovskite thin films. On the other hand, effects from thermal variations due to the functioning of the annealing plates play only a minor role in reproducing the PeLED performance. Although our results are deduced from empirical experimental observations, our findings contribute to the ongoing efforts to better understand the behavior of layered perovskites. They also provide valuable insights for the development of more consistent research methodologies in this field, especially for the newcomers to the domain of perovskite device processing.

2. Materials and Methods

2.1. Materials

Perovskite materials: Phenylethyl Ammonium Bromide (PEABr) and Lead Bromide (PbBr2) were purchased from Sigma-Aldrich (USA). Methyl Ammonium Bromide (MABr) were purchased from DYESOL (Australia). N,N-Dimethylformamide (DMF, > 99.8 %) solvent was purchased from Sigma-Aldrich. 12 mm x 12 mm Indium Tin Oxide (ITO)-coated substrates were purchased from VisionTek Systems Ltd. (UK). Poly(3,4-ethylenedioxythiophene) polystyrene sulfonate (PEDOT:PSS - Al 4083) and 2,2',2''-(1,3,5-Benzinetriyl)-tris(1-phenyl-1-H-benzimidazole) (TPBi, > 99.5 %) were purchased from Ossila (UK). Lithium Fluoride (LiF) (powder, > 99.995 %) was purchased from Sigma-Aldrich. Calcium (Ca, 99.9 %) was purchased from Neyco (France). Silver wires (Ag, 99.9 %) were purchased from GoodFellow Cambridge (UK).

2.2. Device Fabrication

Firstly, patterned ITO-coated glass substrates are cleaned by ultrasonic rinsing in Acetone and Isopropanol subsequently for 15 minutes, and then treated by UV-Ozone for 10 minutes. Secondly, a 50-nm layer of PEDOT:PSS is deposited on the cleaned substrates by spin coating (PEDOT:PSS Al 4083) at 3000 rpm for 50 seconds and annealed at 100 °C for 40 minutes in air. A 1-nm-thin layer of LiF is then deposited by thermal evaporation under a high vacuum on PEDOT:PSS. The samples are then transferred to a nitrogen-filled glovebox for deposition of the perovskite thin films (following the procedures described in the following section). Once the perovskite layers are deposited, the samples are again transferred to thermal evaporators under a vacuum of 10^{-7} mbar to deposit alternately TPBi (35 nm), Ca (40 nm), and Ag electrodes (100 nm) through a shadow mask defining four active areas of 4.53 mm² per substrate.

2.3. Perovskite Deposition

The low-dimensional perovskite precursor is prepared by dissolving PEABr, MABr, and PbBr2 with ratio 0.5:1.2:1.25 in DMF solvent at a molar concentration of 0.5 M. The solution was mixed for at least 24 hours at 50 °C and filtered before deposition. It is then deposited either on UV/Ozone-treated glass substrates or on ITO/PEDOT:PSS/LiF substrates by spin coating at a speed of 7000 rpm. The substrates are then thermally annealed at 90 °C for 15 minutes.

At the beginning of the study, the preparation and deposition of the perovskite precursors are both performed in an MBRAUN UNIlab glovebox workstation filled with nitrogen gas. The content of residual oxygen and moisture inside the workstation is probed using integrated analyzers and maintained at < 10 ppm. The gas purifier of the glovebox is regenerated when there is a significant increase in the H_2O/O_2 concentration (> 100 ppm) or, in normal operating conditions, once every six months.

Then, in the second stage of the research, the precursor solutions are prepared in a separate glovebox (MBRAUN MB200B) before being transferred to the first glovebox for spin-coating. The second glovebox is also nitrogen-filled with a humidity level maintained between 5% and 10% and an O_2 concentration below 1 ppm. Concerning the perovskite deposition, the glovebox is purged with the inert gas one day before the experiment to remove solvent vapor and ensure low H_2O/O_2 concentrations (< 0.01 ppm) during the spin-coating. The temperature of the gloveboxes corresponds to that of the ambient environment.

2.4. Characterizations

The UV-Vis absorption measurements are carried out by a Cary 300 Spectrometer from Agilent Technologies (US). The steady-state and time-resolved photoluminescence (PL) is measured using an FLS980 Spectrometer purchased from Edinburgh Instrument (UK). The AFM measurements are conducted using a Nano-Observer AFM microscope from CSInstruments (Germany). The treatment of collected AFM images is done using the Gwyddion software (http://gwyddion.net/, Czech Republic). In particular, the root-mean-square roughness of the surface is estimated using the embedded roughness tools. Moreover, the surface coverage is obtained by marking the upward crystal grains using the segmentation method before dividing the grain area by the total surface area.

To record the temperature inside the spin-coating chamber, a digital thermometer RS40, with a resolution of 0.1 °C and a measurement rate of 1 Hz, from RS PRO (UK) was used. The current density – luminance – voltage (J-L-V) measurement set-up comprises a calibrated reference Centronic (UK) photodiode (type QD 100-5T with a 100 mm² active area), a sourcemeter Keithley series-2400 fabricated by Keithley Instrument (USA) to supply the LEDs, a Keithley series-2700 multimeter to measure the diode current, a dedicated active amplifier to amplify the intensity (I_{ph}) at the output of the photodiode, and a computer interfaced through Labview to control the voltage source and read the photodiode voltage (V_{ph}) and the current (I) at the output of the multimeter and the source-meter unit. The measurement uncertainties were estimated from the experimental setup: the Keithley error ($\Delta V_{ph}/V_{ph}$) associated with V_{ph} measurement is equal to 5.5%. The error for the load resistance ($\Delta R/R$) is estimated at 0.5%. The accuracy of the photodiode sensitivity at 530 nm ($\Delta\sigma/\sigma$) is approximately 1%. The error on the estimation of the diameter of the LED active area ($\Delta D/D$) is close to 4%. The error on the distance between the LED and the photodiode ($\Delta d/d$) is estimated at 1.2%. Cumulatively, the measurement error on the luminance can be estimated as:

$$(\Delta L/L) = (\Delta V_{ph}/V_{ph}) + (\Delta R/R) + (\Delta\sigma/\sigma) + 2(\Delta D/D) + 2(\Delta d/d) \quad (1)$$

Finally, the global error on the measured luminance is estimated at $\Delta L/L = 17.4$ %.

3. Results and Discussion

3.1. Reproducibility Challenge in PeLEDs Based on Layered Perovskites

This report finds its first justification in our observation of large variations in the performance of our green PeLEDs based on quasi-2D bromide lead perovskites of composition $(PEA)_2MA_{n-1}Pb_nBr_{3n+1}$. The PeLED architecture used a conventional multilayer design [5,13,36]: Indium tin oxide (ITO) (180 nm)/ poly(3,4-ethylenedioxythiophene) polystyrene sulfonate (PEDOT:PSS) (50 nm)/ Lithium fluoride (LiF) (1 nm)/ quasi-2D perovskite (150 nm)/ 2,2′,2″-(1,3,5-Benzinetriyl)-tris(1-phenyl-1-H-benzimidazole) (TPBi) (35 nm)/ Ca (40 nm)/ Ag (100 nm), with the specific addition of an ultrathin LiF layer on top of the PEDOT:PSS hole injection layer to act as an electron blocking layer and a growth template for the halide perovskite [37]. A schematic of the device structure and its corresponding energy band alignment are depicted in Figure S1. We synthesized the perovskite polycrystalline thin films inside a nitrogen-filled glovebox workstation (see Materials and Methods) with controlled O_2 and H_2O concentrations (< 10 ppm), at ambient temperature. We prepared 17 similar perovskite LED devices using the aforementioned conditions. The preparation of the emissive perovskite films was done one after another, with 2 minutes taken for each sample, which involves the time needed to place the substrates on the holder, drop the solution onto the substrates, operate the spin-coater, and transfer the coated samples to the annealing plates. This starting experimental configuration will be referred as Set-up A in the following parts. Additionally, our measurement and calculation of device performance metrics adhered to the LED characterization guideline proposed by Anaya et. al. [38], where the geometry of the inspected LEDs and the photodiodes satisfy the point source assumption. A schematic of our characterization set-up is provided in Figure S2, with a typical estimated experimental error on absolute luminance at 17.4% (see Materials and Methods).

The luminance-voltage and current density-voltage characteristics of the PeLED devices, as shown respectively in Figures 1a and S3, demonstrate a significant standard deviation in all key performance parameters. For instance, the peak luminance (L_{max}) of the PeLEDs occur at different biased voltages ranging between 4.7 V and 8.4 V, with an average value L_{max} of 814 cd/m² and a large standard deviation of 235%, which largely exceeds the margin of the measurement error. The lowest and highest values of L_{max} were recorded at 11 cd/m² and 6,400 cd/m², respectively. Additionally, 3 out of the 17 devices had L_{max} values less than 10 cd/m², indicating non-working devices. Moreover, the values of turn-on voltages (V_{on}) in the device set exhibit a significant variance, varying between 3.2 V and 6.7 V. Similarly, the device efficiency reveals remarkable fluctuations, as evidenced by the statistical data for the maximum external quantum efficiency (EQE) and luminous efficiency (LE) of the devices depicted in Figure 1b.
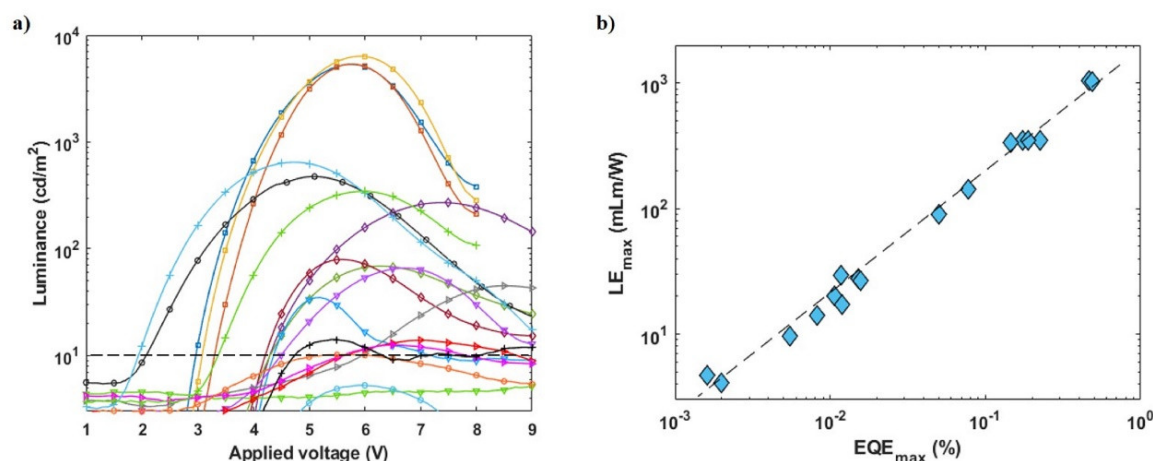
Figure 1. Device performance measured from a set of 17 quasi-2D perovskite LEDs prepared from the standard Set-up A configuration: **a**) Luminance-Voltage curves, where the dotted line indicates the threshold luminance of 10 cd/m^2, and **b**) dispersion of maximum EQE and LE values for the device set. The straight line represents the linear relation between the two quantities.

Due to the low reproducibility observed in our PeLED fabrication, we formulated a hypothesis that the main cause of the variability could be attributed to the perovskite layers. This hypothesis is grounded in the sensitivity of layered perovskite crystallization to synthesis conditions and processing steps, considering that PEDOT:PSS layer, as well as vacuum-evaporated interlayers such as TPBi or Ca, do not show any significant sample-to-sample dispersion (< 5% of standard deviation regarding the thickness, surface roughness, and optical properties) when using similar processing conditions. Accordingly, we examined the optical properties and morphologies of several active perovskite layers processed in our batch. Figure 2a shows the UV-visible absorption and the photoluminescence (PL) of five quasi-2D perovskite thin films deposited in a consecutive 2-minute time frame, using strictly identical experimental parameters. Concerning the optical absorption, several excitonic peaks are identified, each corresponding to a particular n phase (i.e., 402 nm for n=1, 433 nm for n=2, 450 nm for n=3,…. and 520 nm for n=∞). The distribution of these excitonic peaks correlates with the phase composition of the layered perovskite films [39,40]. Here, there is clearly a significant difference in the distribution of the crystallized phases among the five samples, even though they were processed in the same batch from the same mother perovskite precursor solution, employing very similar experimental conditions. In contrast, the PL signals show a similar emission peak around 520 nm with insignificant shifts between the samples, illustrating a cascade energy transfer from the low-n phases toward the high-n phases [17]. Figures 2b and 2c illustrate atomic force microscopy (AFM) morphologies of the first and the last thin films processed in this series: surface roughness and coverage were considerably reduced between the start and end of the process, even though the deposition set-up was unchanged. This result clearly emphasizes the strong impact of extraneous variables occurring in the glovebox environment and which affect the crystallization kinetics of solution-processed layered perovskite thin films, causing, in the end, large variations in PeLED performance.
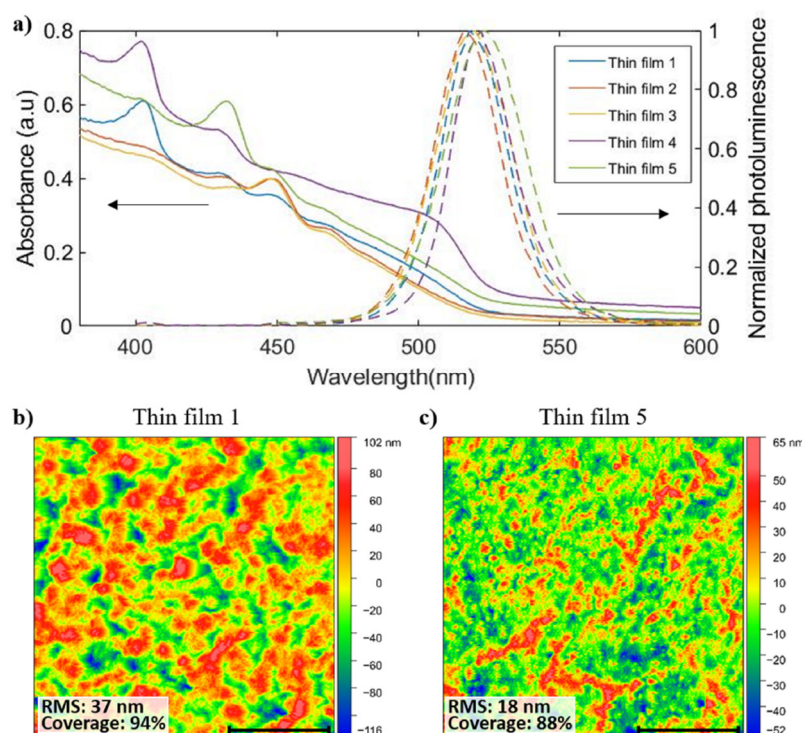
6

Figure 2. a) UV-visible absorption and steady-state PL spectra of intrabatch perovskite thin films deposited successively using Set-up A; b-c) AFM images of the first and the last samples in the batch. The scale bar is 10 µm.

To identify the main factors governing this large deviation, we need to closely focus on the set-ups used for sample preparation. The experimental set-up used to grow perovskite thin films (previously referred as Set-up A) consists of a spin-coater positioned between two hot plates (H1 and H2) that are 20 cm away from each other, for convenient manipulation during the deposition process. H1 functions continuously at a constant temperature of 50 °C for precursor preparation, independent of whether or not a deposition process is currently taking place. Conversely, H2 is only turned on at 90 °C at the beginning of the deposition campaign, for post-deposition annealing purposes. A representation of this configuration is shown in Figure S4. It is also noted that the glovebox is fully regenerated once every 6 months following usual maintenance guidelines. Accordingly, several extraneous factors that could potentially interfere with the kinetics of perovskite crystallization were identified, including:

- Fluctuation in the temperature of the deposition environment;

Thermal instabilities can arise from various sources, including changes in ambient temperature (room temperature) or from the operation of annealing plates H1 and H2 located near the spin-coating chambers. Previous research by Han et al. has shown that changes in room temperature between 21 °C and 31 °C can result in a standard deviation of 70% in the performance of PeLEDs [24]. However, in our experiments, the temperature of the experimental room was maintained between 29 °C and 31 °C using an air conditioning system, and yet the reproducibility of our PeLEDs remained significantly lower than reported by previous studies. While initially considering the fluctuations in the room temperature as a potential explanation, we presume that a 2 °C temperature difference may not entirely account for the low reproducibility rate of our devices. Meanwhile, the operation of annealing plates near the spin-coater could influence the crystallization temperature during the deposition process. Specifically, thermal heating generated by the annealing plates could cause localized temperature increases, potentially favoring the growth process over the nucleation, contributing to the observed variations in morphologies and optical properties, alongside the high roughness of the thin films.

- The presence of a small quantity of uncontrolled O_2 and H_2O inside the glovebox;

Even though the levels of O_2 and H_2O were maintained at a low level (under 10 ppm), which is generally accepted to avoid significant impact on perovskite thin-film formation, fluctuations in their concentration (between 0.1 ppm and 10 ppm) due to natural processes occurring in the glovebox might have also played a role in the poor reproducibility.

- Chemical contamination from evaporated solvents in the glovebox atmosphere;

This could potentially occur when multiple experimentalists share the same deposition glovebox and its set-up, which is very common in academic laboratories. In our experiments, the glovebox was explicitly dedicated to perovskite-related processes, but it was used for various synthesis processes of different perovskite families that required the use of various solvents or antisolvents such as Dimethylformamide (DMF), Dimethyl sulfoxide (DMSO), chlorobenzene, toluene, or diethyl acetate. These solvents and antisolvents could substantially interfere with the crystallization of multi-dimensional perovskites and may dramatically impact their properties.

In the following sections, we try to address and identify the main sources of device inconsistency among these assumptions.

3.2. Effects of Thermal Fluctuation Inside Deposition Chamber and Chemical Contamination on Quasi-2D Perovskite Composition

To test our hypotheses, Set-up A was used as our reference deposition scenario, and we then entailed another deposition configuration referred to as Set-up B. This configuration involves increasing the distance between the spin-coater and the hot plates H1 and H2 to 40 cm and 55 cm, respectively, as shown in Figure S5. In addition, the deposition glovebox is purged with nitrogen gas for approximately an hour, one day prior to the manipulation so that the concentration of residual O_2 and H_2O is always limited below 0.1 ppm. This set-up involves two sub-scenarios that require an examination to assess the effects of chemical contamination: (B1) where the perovskite precursors and solvents are stored within the deposition glovebox (as in Set-up A), and (B2) where the chemical species are stored in a separate glovebox to prevent atmospheric contamination by solvents during film deposition. We then investigated the potential impact of the relative position of the hot plates to the spin coater on the local temperature around the casting samples and its contribution to the observed variations. The temperature, near the sample holder inside the spin-coater, in both Set-ups A and B was monitored, and the thermal fluctuations in both cases are reported in Figure S6. In Set-up A, a slight temperature surge of 0.8 °C was observed, particularly during the first 10 minutes (which is the time window needed to deposit one batch of 4 or 5 devices). Conversely, in Set-up B, the temperature remained practically unaffected, with a gradient of only 0.1 °C. Based on this observation, we concluded that there was a difference in the deposition temperature between Set-up A and B; however, considering the subsidiary variation of temperature in both cases and the accuracy of our temperature probe, we will not discuss the potential impact of such small thermal fluctuation on the emissive layer properties.

Figure 3a displays the UV-visible absorption and PL spectra of 4 intrabatch perovskite thin films with respect to sub-scenario B1. In detail, high excitonic peaks for n=1, n=2, and n=3 phases could be identified in the absorbance spectra of all four samples. More importantly, the consistency in the phase composition is remarkably improved. Likewise, even the minor variations in the PL peaks that have been pointed out in the case of Set-up A are reduced. Also, the kinetics of exciton decay among the four samples were characterized using time-resolved PL measurement, as depicted in Figure S7. In detail, a variation in the average PL decay between 13 ns and 16 ns can be remarked, in which the shorter decay indicates the existence of more non-radiative defects, possibly associated with the thin-film morphology and especially grain size [41].
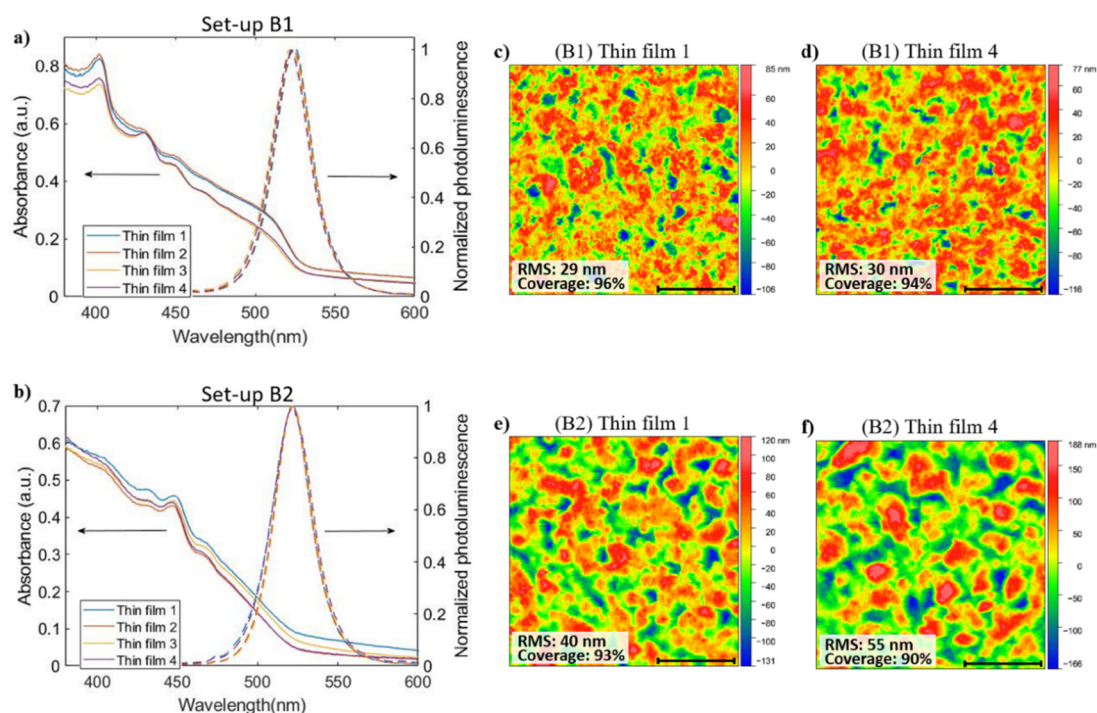
Figure 3. a-b) Absorption and steady-state PL spectra of intrabatch perovskite samples deposited successively using Set-ups B1 and B2; AFM images of the first and the last samples in the batch with respect to **c-d**) Set-up B1 and **e-f**) Set-up B2. The scale bar is 10 μm.

Figures 3c and 3d compare the AFM images of samples 1 and 4, and their surfaces appear to be analogous with a roughness of 29-30 nm and coverage of approximately 95%, explaining their comparable values of PL decay. Subsequently, the improved optical properties of the layered perovskite samples in Set-up B1 compared to Set-up A can be attributed to the better control of oxygen and moisture within the inert atmosphere, owing to the inertisation of the enclosed workstation (i.e., purging the glovebox with fresh nitrogen gas for one hour before the deposition).

The optical properties of intrabatch perovskite thin films synthesized under sub-scenario B2 are also demonstrated in Figure 3b. Firstly, by observing the absorption spectra of the samples, we can identify an identical pattern in the distribution of quasi-2D perovskite domains with a relatively strong peak at 445 nm (corresponding to n=3 phase) while the excitonic peaks originating for n=1 and n=2 phases become less visible. Energetically, in multi-dimensional lead bromide perovskites, a composition with a dominant n=3 phase is usually more beneficial for both efficient PL and electroluminescence (EL) than other compositions [23]. Besides, the PL spectra with the peaks at 520 nm confirm once again the emission from the lowest bandgap phase. Secondly, Figure S8 shows the very strong consistency in the radiative decay kinetics in all four perovskite thin films. For all samples, the average PL lifetime varies around 15.5 ns which is comparable to that of Set-up B1 but inducing clearly less variance. Lastly, the roughness and coverage of the first and fourth samples are shown in Figures 3e and 3f. Compared to the case of Set-up B1, the root-mean-square values are increased considerably, varying between 42 nm to 55 nm, while the surface coverages are in the same order. Moreover, the average grain size, as revealed by AFM mapping, is found to be significantly larger in the case of Set-up B2 compared to Set-up B1. This larger grain size, which is observable for the two intra-batch samples, is responsible for the increased surface roughness in this case. Altogether, this set of data suggests that coherent equipment set-up, careful disposal of chemicals in the glovebox, and regular purification of the deposition environment can promote a more reproducible growth of layered perovskites, allowing for greater uniformity in their morphology and optical properties. Such aspects are likely to be crucial to achieving reproducible optoelectronic devices, as we intend to demonstrate in the last section of this article.

3.3. Improvement in PeLED Reproducibility

Figures 4a and 4b show the luminance-voltage characteristics of two different groups of devices, each of which consists of 14 PeLEDs, corresponding to Set-up B1 and B2, respectively. Obviously, the PeLEDs fabricated using Set-up B2 exhibit the least deviation in key parameters such as turn-on voltage (V_{ON}), maximum visual luminance (L_{max}), or bias voltage at which the luminance peaks, compared to devices in Set-up B1 or Set-up A (as shown in Figure 1). For example, in the deposition scenario B2, V_{ON} only varies within a narrow range from 3 V to 3.8 V as well as most of the luminance curves reach their peaks around 6V. Although the improvement is less pronounced in Set-up B1, it still yields better consistency in device performance when compared to the reference Set-up A. Furthermore, Figure 4c statistically illustrates the distribution of L_{max} values across all PeLEDs with respect to the three deposition scenarios. It is clear that, while the mean values of L_{max} in all three cases are in the same order of magnitude (approximately 1,000 cd/m²), the variance has been noticeably reduced when switching from Set-up A (standard deviation of 235%) to Set-up B1 (standard deviation of 76%) and Set-up B2 (standard deviation of 38%).
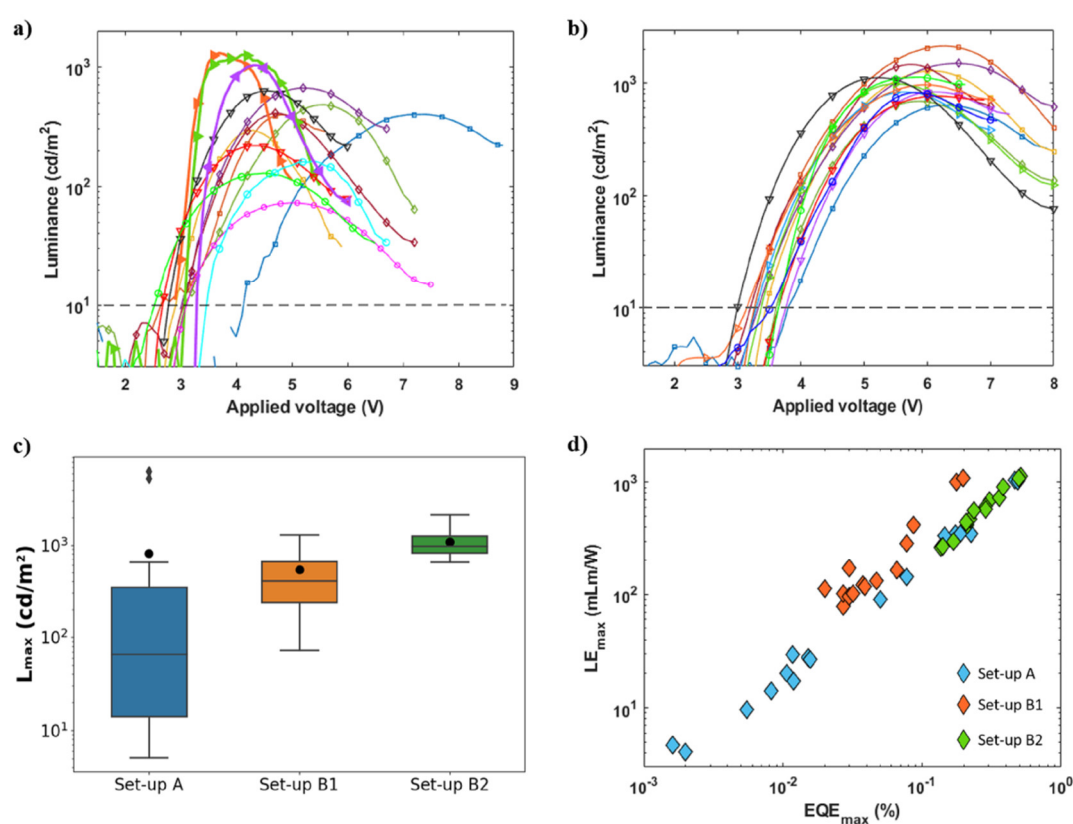
Figure 4. Luminance-Voltage curves of two sets of 14 PeLEDs corresponding to (**a**) Set-up B1 and (**b**) Set-up B2; (**c**) Statistical distribution of the luminance peaks of these devices, compared to those in Set-up A. The whiskers represent the upper and lower quartiles, the diamond markers represent the outliers, the middle lines represent the median value, and the black dots represent the mean value of each dataset; (**d**) maximum EQE versus maximum LE of all devices fabricated using Set-ups A, B1, and B2.

Concerning the device efficiency, Figures 4d and S9 portray the statistical variability in both maximal external quantum efficiency (EQE_{max}) and maximal luminous efficiency (LE_{max}) for all devices. Similar to the observed results when examining the device's luminance, it is evident that the mean values of these parameters amongst the three experimental scenarios are comparable, with a slight improvement when utilizing a different glovebox to store the perovskite-related solvents and antisolvents (Set-up B2). More importantly, the most noteworthy improvement lies in the reproducibility of device efficiency by altering the deposition set-ups. Specifically, by employing Set-

up B2, we have achieved a deviation in EQE_{max} as low as 42%, representing a decrease of over 3 folds compared to the utilization of the original set-up A.

This result suggests that the fluctuation in concentration of oxygen and moisture during the perovskite spin-coating and annealing, as well as untraceable chemical contamination in the deposition environment, can negatively affect the crystallization of the perovskites and therefore diminishes the reproducibility of the corresponding PeLEDs. It is worth noting that, these small variations in the extraneous conditions of the experimental set-up are usually considered insignificant and often neglected in the literature; however, we emphasize the importance of controlling such factor in the deposition of quasi-2D perovskites. As a result, we have succeeded in minimizing the deviations in the key performance parameters to approximately 40%. This improvement could be assigned to the consistency in the phase domain distribution and the morphology of the perovskite layers that have been discussed above. Before concluding this report, it is essential to note that this value of uncertainty still surpasses the inherent margin of error of our measurement system (~18%), implying the influences of additional factors beyond those studied in this article, such as the temperature changes due to hot plate functioning or the deposition of the ultra-thin LiF layer, and the need to further optimize controllable variables in our perovskite deposition process.

4. Conclusions

This report outlines the crucial importance of controlling extraneous glovebox-related variables in the fabrication of PeLEDs based on quasi-2D perovskites to achieve high device-to-device reproducibility. Particularly, we have demonstrated the effects of varying oxygen and moisture levels and chemical pollution inside a deposition glovebox on the consistent formation of the quasi-2D phases as well as on the homogeneity of surface morphology. Indeed, such problem has been recognized by researchers but only until now, it is well understood to what extent it may deteriorate the device performance. In addition, it is advisable to have a careful arrangement of equipment used during the deposition in order to maintain a high reproducibility of the experiment. Subsequently, it has been shown that, with mindful attention to keeping the glovebox atmosphere as clean as possible thanks to regular purifications, the uncertainty of our PeLED fabrication process decreases significantly from 230% to 38% with regard to device's maximum brightness or from 140% to 42% when considering device's EQE. Not only this best practice can be applied to the study of PeLEDs but it may also be considered for other types of optoelectronic devices based on layered perovskites, such as solar cells and photodetectors. Lastly, considering the large diversity of configurations between laboratories or between industrial actors, we point out that all experimental details, even those which seem trivial or irrelevant to the process, are crucial to ensure reproducible performance which can be compared by different researchers and groups in the broad and dynamic halide perovskite community.

Conflicts of Interest: The authors declare no conflicts of interest. The funders had no role in the design of the study; in the collection, analyses, or interpretation of data; in the writing of the manuscript; or in the decision to publish the results.

References

1. Jena, A.K.; Kulkarni, A.; Miyasaka, T. Halide Perovskite Photovoltaics: Background, Status, and Future Prospects. Chem. Rev. 2019, 119, 3036–3103, doi:10.1021/acs.chemrev.8b00539.
2. Chen, X.; Zhou, H.; Wang, H. 2D/3D Halide Perovskites for Optoelectronic Devices. Frontiers in Chemistry 2021, 9.
3. Wang, H.-P.; Li, S.; Liu, X.; Shi, Z.; Fang, X.; He, J.-H. Low-Dimensional Metal Halide Perovskite Photodetectors. Ad-vanced Materials 2021, 33, 2003309, doi:10.1002/adma.202003309.
4. Liu, X.-K.; Xu, W.; Bai, S.; Jin, Y.; Wang, J.; Friend, R.H.; Gao, F. Metal Halide Perovskites for Light-Emitting Diodes. Nat. Mater. 2021, 20, 10–21, doi:10.1038/s41563-020-0784-7.
5. Fakharuddin, A.; Gangishetty, M.K.; Abdi-Jalebi, M.; Chin, S.-H.; bin Mohd Yusoff, A.R.; Congreve, D.N.; Tress, W.; Deschler, F.; Vasilopoulou, M.; Bolink, H.J. Perovskite Light-Emitting Diodes. Nat Electron 2022, 5, 203–216, doi:10.1038/s41928-022-00745-7.
6. Quan, L.N.; Rand, B.P.; Friend, R.H.; Mhaisalkar, S.G.; Lee, T.-W.; Sargent, E.H. Perovskites for Next-Generation Op-tical Sources. Chem. Rev. 2019, 119, 7444–7477, doi:10.1021/acs.chemrev.9b00107.
7. Zhang, S.; Yi, C.; Wang, N.; Sun, Y.; Zou, W.; Wei, Y.; Cao, Y.; Miao, Y.; Li, R.; Yin, Y.; et al. Efficient Red Perovskite Light-Emitting Diodes Based on Solution-Processed Multiple Quantum Wells. Advanced Materials 2017, 29, 1606600, doi:10.1002/adma.201606600.
8. Kumar, S.; Jagielski, J.; Kallikounis, N.; Kim, Y.-H.; Wolf, C.; Jenny, F.; Tian, T.; Hofer, C.J.; Chiu, Y.-C.; Stark, W.J.; et al. Ultrapure Green Light-Emitting Diodes Using Two-Dimensional Formamidinium Perovskites: Achieving Recommendation 2020 Color Coordinates. Nano Lett. 2017, 17, 5277–5284, doi:10.1021/acs.nanolett.7b01544.
9. Hou, S.; Gangishetty, M.K.; Quan, Q.; Congreve, D.N. Efficient Blue and White Perovskite Light-Emitting Diodes via Manganese Doping. Joule 2018, 2, 2421–2433, doi:10.1016/j.joule.2018.08.005.
10. Adjokatse, S.; Fang, H.-H.; Loi, M.A. Broadly Tunable Metal Halide Perovskites for Solid-State Light-Emission Applications. Materials Today 2017, 20, 413–424, doi:10.1016/j.mattod.2017.03.021.
11. Tan, Z.-K.; Moghaddam, R.S.; Lai, M.L.; Docampo, P.; Higler, R.; Deschler, F.; Price, M.; Sadhanala, A.; Pazos, L.M.; Credgington, D.; et al. Bright Light-Emitting Diodes Based on Organometal Halide Perovskite. Nature Nanotech 2014, 9, 687–692, doi:10.1038/nnano.2014.149.
12. Sheng, X.; Li, Y.; Xia, M.; Shi, E. Quasi-2D Halide Perovskite Crystals and Their Optoelectronic Applications. J. Mater. Chem. A 2022, 10, 19169–19183, doi:10.1039/D2TA02219B.
13. Zhang, L.; Sun, C.; He, T.; Jiang, Y.; Wei, J.; Huang, Y.; Yuan, M. High-Performance Quasi-2D Perovskite Light-Emitting Diodes: From Materials to Devices. Light Sci Appl 2021, 10, 61, doi:10.1038/s41377-021-00501-0.
14. Zou, C.; Zhang, C.; Kim, Y.-H.; Lin, L.Y.; Luther, J.M. The Path to Enlightenment: Progress and Opportunities in High Efficiency Halide Perovskite Light-Emitting Devices. ACS Photonics 2021, 8, 386–404, doi:10.1021/acsphotonics.0c01394.
15. Chen, P.; Bai, Y.; Lyu, M.; Yun, J.-H.; Hao, M.; Wang, L. Progress and Perspective in Low-Dimensional Metal Halide Perovskites for Optoelectronic Applications. Solar RRL 2018, 2, 1700186, doi:10.1002/solr.201700186.

16. Yantara, N.; Bruno, A.; Iqbal, A.; Jamaludin, N.F.; Soci, C.; Mhaisalkar, S.; Mathews, N. Designing Efficient Energy Funneling Kinetics in Ruddlesden–Popper Perovskites for High-Performance Light-Emitting Diodes. Advanced Materials 2018, 30, 1800818, doi:10.1002/adma.201800818.

17. Yuan, M.; Quan, L.N.; Comin, R.; Walters, G.; Sabatini, R.; Voznyy, O.; Hoogland, S.; Zhao, Y.; Beauregard, E.M.; Kanjanaboos, P.; et al. Perovskite Energy Funnels for Efficient Light-Emitting Diodes. Nature Nanotech 2016, 11, 872–877, doi:10.1038/nnano.2016.110.

18. Byun, J.; Cho, H.; Wolf, C.; Jang, M.; Sadhanala, A.; Friend, R.H.; Yang, H.; Lee, T.-W. Efficient Visible Quasi-2D Perovskite Light-Emitting Diodes. Advanced Materials 2016, 28, 7515–7520, doi:10.1002/adma.201601369.

19. Sun, C.; Jiang, Y.; Cui, M.; Qiao, L.; Wei, J.; Huang, Y.; Zhang, L.; He, T.; Li, S.; Hsu, H.-Y.; et al. High-Performance Large-Area Quasi-2D Perovskite Light-Emitting Diodes. Nat Commun 2021, 12, 2207, doi:10.1038/s41467-021-22529-x.

20. Liu, Z.; Qiu, W.; Peng, X.; Sun, G.; Liu, X.; Liu, D.; Li, Z.; He, F.; Shen, C.; Gu, Q.; et al. Perovskite Light-Emitting Diodes with EQE Exceeding 28% through a Synergetic Dual-Additive Strategy for Defect Passivation and Nanostructure Regulation. Advanced Materials 2021, 33, 2103268, doi:10.1002/adma.202103268.

21. Han, T.-H.; Jang, K.Y.; Dong, Y.; Friend, R.H.; Sargent, E.H.; Lee, T.-W. A Roadmap for the Commercialization of Perovskite Light Emitters. Nat Rev Mater 2022, 7, 757–777, doi:10.1038/s41578-022-00459-4.

22. Xing, J.; Zhao, Y.; Askerka, M.; Quan, L.N.; Gong, X.; Zhao, W.; Zhao, J.; Tan, H.; Long, G.; Gao, L.; et al. Col-or-Stable Highly Luminescent Sky-Blue Perovskite Light-Emitting Diodes. Nat Commun 2018, 9, 3541, doi:10.1038/s41467-018-05909-8.

23. Laxmi; Kabra, D. Optimization of Composition with Reduced Phase Impurity in Quasi-2D Perovskite for Elec-troluminescence. Advanced Photonics Research 2021, 2, 2000164, doi:10.1002/adpr.202000164.

24. Han, Y.; Wang, J.; Bischak, C.G.; Kim, S.; Lee, K.; Shin, D.; Lee, M.J.; Ginger, D.S.; Hwang, I. Significance of Ambient Temperature Control for Highly Reproducible Layered Perovskite Light-Emitting Diodes. ACS Photonics 2020, 7, 2489–2497, doi:10.1021/acsphotonics.0c00779.

25. Bae, Y.; Ryu, J.; Yoon, S.; Kang, D.-W. Recent Progress in Quasi-Two-Dimensional and Quantum Dot Perovskite Light-Emitting Diodes Harnessing the Diverse Effects of Ligands: A Review. Nano Res. 2022, 15, 6449–6465, doi:10.1007/s12274-022-4252-3.

26. Yang, X.; Zhang, X.; Deng, J.; Chu, Z.; Jiang, Q.; Meng, J.; Wang, P.; Zhang, L.; Yin, Z.; You, J. Efficient Green Light-Emitting Diodes Based on Quasi-Two-Dimensional Composition and Phase Engineered Perovskite with Surface Passivation. Nat Commun 2018, 9, 570, doi:10.1038/s41467-018-02978-7.

27. Ye, Z.; Xia, J.; Zhang, D.; Duan, X.; Xing, Z.; Jin, G.; Cai, Y.; Xing, G.; Chen, J.; Ma, D. Efficient Quasi-2D Per-ovskite Light-Emitting Diodes Enabled by Regulating Phase Distribution with a Fluorinated Organic Cation. Nanomaterials 2022, 12, 3495, doi:10.3390/nano12193495.

28. Cheng, T.; Qin, C.; Watanabe, S.; Matsushima, T.; Adachi, C. Stoichiometry Control for the Tuning of Grain Passivation and Domain Distribution in Green Quasi-2D Metal Halide Perovskite Films and Light-Emitting Diodes. Ad-vanced Functional Materials 2020, 30, 2001816, doi:10.1002/adfm.202001816.

29. Yuan, Z.; Miao, Y.; Hu, Z.; Xu, W.; Kuang, C.; Pan, K.; Liu, P.; Lai, J.; Sun, B.; Wang, J.; et al. Unveiling the Synergistic Effect of Precursor Stoichiometry and Interfacial Reactions for Perovskite Light-Emitting Diodes. Nat Commun 2019, 10, 2818, doi:10.1038/s41467-019-10612-3.

30. Chen, C.; Zeng, L.; Jiang, Z.; Xu, Z.; Chen, Y.; Wang, Z.; Chen, S.; Xu, B.; Mai, Y.; Guo, F. Vacuum-Assisted Preparation of High-Quality Quasi-2D Perovskite Thin Films for Large-Area Light-Emitting Diodes. Advanced Functional Materials 2022, 32, 2107644, doi:10.1002/adfm.202107644.

31. Wang, J.; Li, D.; Mu, L.; Li, M.; Luo, Y.; Zhang, B.; Mai, C.; Guo, B.; Lan, L.; Wang, J.; et al. Inkjet-Printed Full-Color Matrix Quasi-Two-Dimensional Perovskite Light-Emitting Diodes. ACS Appl. Mater. Interfaces 2021, 13, 41773–41781, doi:10.1021/acsami.1c07526.

32. Zhang, M.; Yuan, F.; Zhao, W.; Jiao, B.; Ran, C.; Zhang, W.; Wu, Z. High Performance Organo-Lead Halide Perovskite Light-Emitting Diodes via Surface Passivation of Phenethylamine. Organic Electronics 2018, 60, 57–63, doi:10.1016/j.orgel.2018.05.026.

33. Ma, J.; Yang, L.; Zhang, Y.; Kuang, Y.; Shao, M. Rearranging the Phase Distribution of Quasi-2D Perovskite for Efficient and Narrow Emission Perovskite Light-Emitting Diodes. J. Phys. Chem. Lett. 2022, 13, 4739–4746, doi:10.1021/acs.jpclett.2c01059.

34. Worku, M.; He, Q.; Xu, L.; Hong, J.; Yang, R.X.; Tan, L.Z.; Ma, B. Phase Control and In Situ Passivation of Quasi-2D Metal Halide Perovskites for Spectrally Stable Blue Light-Emitting Diodes. ACS Appl. Mater. Interfaces 2020, 12, 45056–45063, doi:10.1021/acsami.0c12451.

35. Molenda, Z.; Chambon, S.; Bassani, D.M.; Hirsch, L. Assessing the Impact of Ambient Fabrication Temperature on the Performance of Planar CH3NH3PbI3 Perovskite Solar Cells. European Journal of Inorganic Chemistry 2021, 2021, 2533–2538, doi:10.1002/ejic.202100329.

36. Ji, K.; Anaya, M.; Abfalterer, A.; Stranks, S.D. Halide Perovskite Light-Emitting Diode Technologies. Advanced Optical Materials 2021, 9, 2002128, doi:10.1002/adom.202002128.

37. Zhao, B.; Lian, Y.; Cui, L.; Divitini, G.; Kusch, G.; Ruggeri, E.; Auras, F.; Li, W.; Yang, D.; Zhu, B.; et al. Efficient Light-Emitting Diodes from Mixed-Dimensional Perovskites on a Fluoride Interface. Nat Electron 2020, 3, 704–710, doi:10.1038/s41928-020-00487-4.

38. Anaya, M.; Rand, B.P.; Holmes, R.J.; Credgington, D.; Bolink, H.J.; Friend, R.H.; Wang, J.; Greenham, N.C.; Stranks, S.D. Best Practices for Measuring Emerging Light-Emitting Diode Technologies. Nat. Photonics 2019, 13, 818–821, doi:10.1038/s41566-019-0543-y.

39. Mai, C.; Cun, Y.; Luo, Y.; Zhang, B.; Li, M.; Li, H.; Mu, L.; Wang, J.; Li, D.; Wang, J. Dependence of the Radiative Efficiency of Quasi-2D Perovskite Light-Emitting Diodes on the Multiquantum-Well Composition. J. Phys. Chem. C 2021, 125, 12241–12250, doi:10.1021/acs.jpcc.1c03458.

40. Yan, C.; Lin, K.; Lu, J.; Wei, Z. Composition Engineering to Obtain Efficient Hybrid Perovskite Light-Emitting Diodes. Front. Optoelectron. 2020, 13, 282–290, doi:10.1007/s12200-020-1046-7.

41. Li, Z.; Cao, K.; Li, J.; Du, X.; Tang, Y.; Yu, B. Modification of Interface between PEDOT:PSS and Perovskite Film Inserting an Ultrathin LiF Layer for Enhancing Efficiency of Perovskite Light-Emitting Diodes. Organic Electronics 2020, 81, 105675, doi:10.1016/j.orgel.2020.105675.